bioRxiv preprint doi: https://doi.org/10.1101/2020.06.19.160861; this version posted June 20, 2020. The copyright holder for this preprint (which was not certified by peer review) is the author/funder, who has granted bioRxiv a license to display the preprint in perpetuity. It is made available under aCC-BY-NC-ND 4.0 International license.

The Structure-Based Virtual Screening for Natural Compounds that Bind with the Activating Receptors of Natural Killer Cells

Adekunle Babajide Rowaiye[1,2], Solomon Oni[*1], Ikemefuna Chijioke Uzochukwu[3], Alex Akpa[1], Charles Okechukwu Esimone[2]

[1]*Department of Medical Biotechnology, National Biotechnology Development Agency, Abuja, Nigeria*

[2]*Department of Pharmaceutical Microbiology and Biotechnology, Faculty of Pharmaceutical Sciences, Nnamdi Azikiwe University, Anambra State, Nigeria*

[3]*Department of Pharmaceutical and Medicinal Chemistry, Faculty of Pharmaceutical Sciences, Nnamdi Azikiwe University, Anambra State, Nigeria.*

Abstract

Aim: This study is aimed at prospecting for natural compounds that have strong binding affinity for the Activating Receptors of Natural Killer (NK) cells.

B**ackground:** NK cells are responsible for the immunosurveillance of tumor and virally- infected cells. The cytotoxic potentials of this unique population of immune cells are triggered by the activating receptors. Through ligand-binding, these receptors induce the tyrosine phosphorylation of adapter proteins through their Immunoreceptor Tyrosine–based Activation Motif ITAM sequences and this triggers direct cytotoxicity and the production of cytokines through different signal pathways.

Objective: To computationally predict the selectivity, specificity, and efficacy of natural compounds to be used as immunostimulatory agents for cancer treatment.

Method: In this study, 1,697 natural compounds were obtained from 82 edible tropical plants through data mining. The molecular docking simulations of these compounds were executed against 18 activating NK cells receptor targets using the Python Prescription 0.8. An arbitrary docking score ≥ -7.0 kcal/mol was chosen as cut off value. Further screening for oral bioavailability, promiscuity, molecular complexity and pharmacokinetic properties using the Swissadme and pkCSM webservers. The ligand similarity analysis and phylogenetic analysis of the receptors was carried out with the ChemMine and Clustal Omega webservers respectively. Binding site analyses and bioactivity prediction were also done with the Protein-Ligand Interaction Profiler and Molinspiration webservers respectively. Normal mode analyses were carried out with the CABS-flex 2.0 server.

Result: Seventeen bioactive and non-promiscuous lead compounds with good physicochemical and pharmacokinetic properties were identified.

Conclusion: Further tests are required to evaluate the efficacy of the lead compounds.

Key words: Cytotoxic, Activating Receptors, Ligands, Cytokines, Immunoreceptor Tyrosine–based Activation Motif

[*] Address correspondence to the Department of Medical Biotechnology,
National Biotechnology Development Agency,
Abuja 900101, Nigeria. Tel: +2347032283653; Email: goodnessoni@gmail.com

bioRxiv preprint doi: https://doi.org/10.1101/2020.06.19.160861; this version posted June 20, 2020. The copyright holder for this preprint (which was not certified by peer review) is the author/funder, who has granted bioRxiv a license to display the preprint in perpetuity. It is made available under aCC-BY-NC-ND 4.0 International license.

1.0 INTRODUCTION

Cancer is a group of diseases characterized by erratic cell growth which invade and spread into other parts of the body [1, 2]. They are caused by DNA damage and an ineffective DNA repair mechanism. According to a 2015 WHO report, Cancer is the second leading cause of death globally and there were 90.5 million incidences of cancer in 2015 which accounted for 8.8 million deaths [3].

Cancers are caused by a persistent damage to DNA which culminates into mutations of certain gene sequences in the human genome [4]. Expression of these mutant sequences lead to an autonomous and unregulated hyper-proliferation of cells; insufficient apoptosis; altered differentiation and metabolism; genomic instability and immortalization [5]. The abnormal proliferation of cells is due to alterations in the cell cycle replication mechanism due to nuclear and cytoplasm distortions. These changes include hyperchromatism, increased telomerase expression, prominent nucleoli, irregular chromatin distribution within nuclei, and increased size of nucleus, pleomorphism, and chromosomal translocations [6,7].

Available cancer therapies such as chemotherapy are non-selective as other normal rapidly dividing cells (including immune cells) are destroyed. Another major frustration faced by clinicians and researchers includes the evasive nature of cancer cells as they beat the immune system by their molecular 'anonymity'. This is further complicated by their rapid multiplication, invasiveness and malignant abilities. Through intricate mechanisms, the rapidly dividing aberrant cells are able to evade the immune system, invade the surrounding tissue and enter into the lymph nodes and metastasize [8]. Therefore, the development of potential therapeutic agents must consider selectivity, specificity, and efficacy.

NK cells are responsible for immune-surveillance of tumor and virally infected cells. To unlock or lock the cytotoxic potentials of this unique population of immune cells are activating and inhibiting receptors respectively. The immunomodulatory potential of NK cells guarantees that the immune system does not fight against itself. Therefore, NK targeted therapies hold great promise in the treatment of cancers.

bioRxiv preprint doi: https://doi.org/10.1101/2020.06.19.160861; this version posted June 20, 2020. The copyright holder for this preprint (which was not certified by peer review) is the author/funder, who has granted bioRxiv a license to display the preprint in perpetuity. It is made available under aCC-BY-NC-ND 4.0 International license.

CHAPTER 2: MATERIALS AND METHODS

2.1 Materials

The protein and ligand databases used were: Protein Databank, Uniprot, and PubChem. The webservers used were: pkCSM, Clustal Omega, ExPASy, Molinspiration, Protein-Ligand Interaction Profiler (PLIP), SWISS-MODEL, Swissadme, ChemMine, MolProbity, Chiron and CABS-flex 2.0. The softwares used were: Discovery studio 2017, Open babel, Pymol, and Python prescription (PyRx) 0.8.

2.2. Methods

2.2.1 Identification of targets: The activating receptors of NK cells were identified by an extensive literature review. Validation of these molecular targets was also by empirical evidences provided by relevant research publications. The 3D crystallographic structures of these proteins were downloaded from the RCSB protein databank in the pdb format and visualized using the Pymol software [9]. The homology modeling of the proteins whose structures could not be obtained in the RCSB protein databank was executed using the SWISS-MODEL web-server [10]. The templates of closely related proteins were used for the modeling as seen in Table 1.

2.2.2 Analysis and validation of protein structures: An all-atom structural validation and dihedral-angle diagnostics of the protein crystallography was conducted using the online server, MolProbity and the Ramanchandran plots were also obtained as seen in Table 2 [11].

2.2.3 Preparation of protein targets for docking: In preparing the protein targets for molecular docking, all available water molecules, native ligands and unwanted chains were removed using the Pymol software [9]. Energy minimization of the protein targets to resolve steric clashes was done using online tool, *Chiron* as seen in Table 3 [12]. The PyRx software was used to convert the protein targets from pdb to pdbqt files [13].

2.2.4 Building of library of natural bioactive compounds: A library of 1,697 compounds was built from an extensive data mining from the literature review of 79 plants (See supplementary data) predominantly found in Nigeria and tropical Africa. The 3D structures of these natural compounds were downloaded from the PubChem chemical database in their SDF format [14]. The properties of these compounds such as molecular weight, canonical SMILES, number of heavy atoms, hydrogen bond donors, hydrogen bond acceptors, Log P and topological polar surface area were obtained from Pubchem [14].

bioRxiv preprint doi: https://doi.org/10.1101/2020.06.19.160861; this version posted June 20, 2020. The copyright holder for this preprint (which was not certified by peer review) is the author/funder, who has granted bioRxiv a license to display the preprint in perpetuity. It is made available under aCC-BY-NC-ND 4.0 International license.

2.2.5 Preparation for docking: Prior to docking, 1697 natural compounds were screened for bioavailability using the Lipinski and Veber rules. As stated by Lipinski, the drug-like properties include

a MW ≥ 500, Hydrogen Bond Donor ≥ 10, Hydrogen Bond Acceptor ≥ 5 and a Log P value ≥ 5. Further screening was done for cellular permeability using the Veber's rule. Only compounds of Topological Polar Surface Area (TPSA) values of ≥ 140 and number of rotatable bonds ≥ 10 were successful [28, 29].

The docking protocol was validated by using a structure from the Protein Data Bank. The molecule which is the Adhesion Domain of Human CD2 (PDB ID: 1GYA) was downloaded in pdb format and separated from N-Glycan which is the native ligand. The separated molecules were docked together using PyRx 0.8. The docked result was superimposed on the pure protein structure and compared with the original 1GYA structure found in the data bank (Figure 1).

Ligands were uploaded unto PyRx 0.8 through the Open babel plug-in. For stable conformation, the conjugate gradient descent was used as optimization algorithm. The Universal Force Field (UFF) was used as the energy minimization parameter.

The Spatial Data File (SDF) formats of all ligands were converted to the pdbqt format in readiness for docking. The grids were maximized to cover the entire binding site of the ligand. Molecular docking of ligands against protein targets was executed through AutoDock Vina plug-in of the PyRx software. Based on the scoring function, the best fits were obtained and saved in excel files.

2.2.6 Screening for potency: The first stage of the screening was for drug potency. Molecular docking was used as the first step in the virtual screening process and the docking scores were used as empirical predictors of the strength of the intermolecular interactions between the receptors and the ligands (See supplementary data).

A uniform docking scoring cutoff of -7.0 kcal/mol was used to serve as a general border line for the binding energies obtained between the receptors and the ligands. Because drug potency is an aggregate of the binding affinity and the efficacy, further screening for efficacy was executed by imploring the use of three Ligand Efficiency Metrics (LEM) which are the Ligand Efficiency (LE), ligand-efficiency-dependent lipophilicity, (LELP) and Ligand-lipophilicity efficiency (LLE). The LE was calculated as the binding energy divided by the number of heavy atoms; the LELP is the Log P value of the ligand divided by the LE; and the LLE is the binding energy minus the log P. The cut offs are ≥ 0.3 for LE; -10 to 10 for LELP; and ≥ 5.0 for LLE (See supplementary data for results).

2.2.7 Further screening for Oral Bioavailability, Promiscuity and pharmacokinetic properties: After the initial screening for drug likeness using the Lipinski and Veber rules, the natural compounds were screened for saturation and promiscuity using the SWISSADME webserver [15]. Using the canonical

bioRxiv preprint doi: https://doi.org/10.1101/2020.06.19.160861; this version posted June 20, 2020. The copyright holder for this preprint (which was not certified by peer review) is the author/funder, who has granted bioRxiv a license to display the preprint in perpetuity. It is made available under aCC-BY-NC-ND 4.0 International license.

SMILES, a Quantitative-Structural Activity Relationship (QSAR) based prediction of the Absorption, Distribution, Metabolism, Excretion and Toxicity (ADMET) properties of the selected compounds was executed using the pkCSM and this was used for further screening. (See supplementary data for results).

2.2.8: Prediction of Bioactivity: Using the Molinspiration webserver, the bioactivity of the compounds was predicted as seen in Table 10.

2.2.9: Specificity/promiscuity analyses: After the initial screenings, the comparative binding affinity analysis of all the protein-ligand interactions was done to check for specific and promiscuous binding (Table 11).

2.2.10 Structural similarity analyses: The similarity analyses of all the screened ligands were done using the *ChemMine* webserver as shown in Table 12 [16]. A structural analysis of the protein targets was done through a pairwise Percent Identity Matrix. The results are seen in Table 13. A multiple sequence alignment of the amino acid residues of the extracellular domain of all the receptor targets and subsequently the phylogenetic analysis was done using the Clustal Omega webserver [17]. The results are shown in Figure 2.

2.2.11: Binding Site analyses: The poses of the selected ligands as they interact with the receptors during docking were saved on PyRx and viewed on PyMol. The protein structures were superimposed on PyMol and saved in the pdb format. The structures were uploaded into the Protein-Ligand Interaction Profiler (PLIP) webserver for the analysis of their binding sites [18]. The summary of all the protein-ligand interactions are shown in supplementary data.

2.2.12: Normal Mode Analysis: The Root Mean Square Fluctuation (RMSF) plots of the amino acid residues of native and mutant (after binding with ligand) proteins were obtained using the CABS-flex 2.0 webserver (Table 14) [19].

3.0 RESULTS AND DISCUSION

3.1 Preparation for docking

3.1.1 Profiling and homology modeling of the protein structures: From Table 1, the four proteins modeled have very high percentage (between 85.96 and 92.44%) similarity with their templates. Usually, protein structures with over 30% identity to their templates can be predicted with an accuracy equivalent to a low-resolution X-ray structure [20]. In such high sequence identities, the major errors in modeling arise from the use of a poor template and inaccurate alignment of target-template sequence [21].

bioRxiv preprint doi: https://doi.org/10.1101/2020.06.19.160861; this version posted June 20, 2020. The copyright holder for this preprint (which was not certified by peer review) is the author/funder, who has granted bioRxiv a license to display the preprint in perpetuity. It is made available under aCC-BY-NC-ND 4.0 International license.

Table 1: Homology modeling of the proteins

S/N	Receptor name	Uniprot code	Template	% Similarity with template
1	Killer cell immunoglobulin-like receptor 2DS1	Q14954	KIR3DL1	92.44
2	Killer cell immunoglobulin-like receptor 2DS3	Q14952	KIR3DL1	88.36
3	Killer cell immunoglobulin-like receptor 2DS5	Q14953	KIR2DL1	91.96
4	NKG2-E type II integral membrane protein	Q07444	NKG2A	85.96

3.1.2 Ramachandran Analysis: The ramanchandran plot was used to validate the macromolecular crystal structures of all the receptor targets to be studied by revealing the torsional conformation of their amino acids. From Table 2, all the protein structures have over 80% and 90% of their residues within the favoured and allowed regions respectively signifying good stereochemical quality. None of the proteins are intrinsically-disordered because of the chemical correctness of the torsional angles of their backbone [22].

When the φ and ψ angles are combined, an outlier residue has unusual torsional angles. All the protein structures had ramachandran outliers less than 0.05% signifying quality backbone conformation [23]. In this regard, the two proteins of least structural quality are KIR2DS1 and KIR2DS3 with 9 (0.046%) and 7 (0.036%) outliers respectively. These two proteins were homologically modeled from the same template, KIR3DL1. The relatively higher percentage of outliers found in these two proteins may be due to partially disordered large loops in the template. Loops have high electronic densities due to their structural flexibility and randomness and hence their residues show a broader range of dihedral angle values [24].

Though from Table 2, all the 18 proteins meet the required cut-off, IL15Rα and CD2 have the highest and lowest structural quality respectively. This difference is due to the method used for the structural analysis of these proteins. The structure of IL15Rα (pdb 4gs7) was obtained from x-ray crystallography, while CD2 (pdb1gya) was obtained from solution nuclear magnetic resonance (NMR). NMR gives a lesser resolving power than X-ray crystallography because it offers much more complex information from the same material. Most successful computational protein design use high-resolution X-ray crystallographic structures as templates [25].

bioRxiv preprint doi: https://doi.org/10.1101/2020.06.19.160861; this version posted June 20, 2020. The copyright holder for this preprint (which was not certified by peer review) is the author/funder, who has granted bioRxiv a license to display the preprint in perpetuity. It is made available under aCC-BY-NC-ND 4.0 International license.

Table 2: Ramanchandran Plot Analysis of Protein Structures

S/N	Receptor	Favoured Region (98%)	Allowed Region (>99.8%)	No of Outliers (%)	Outlier Residues
1	CD2	81.6% (84/103)	96.1% (99/103)	4 (0.039)	8 GLU (-57.8, 91.6)
					27 SER (-167.0, -50.7)
					52 GLU (-177.9, 85.5)
					72 HIS (61.8, 110.6)
2	NCR2	94.3 (100/106)	98.1(104/106)	2 (0.019)	59 TRP (-73.2, -140.7)
					60 THR (97.5, 67.6)
3	KIR2DS2	95.3% (182/191)	97.9% (187/191)	4(0.021)	57 ASP (-66.3, 48.6)
					67 GLY (-29.0, 164.6)
					68 PRO (-33.4, 118.0)
					114 PRO (-61.5, -70.2)
4	NCR1	94.1% (175/186)	98.9% (184/186)	2 (0.011)	100 TYR (60.2, -94.5)
					150 VAL (69.5, -34.2)
5	IL2Rα	86.3% (101/117)	96.6% (113/117)	4 (0.034)	22 GLU (-46.7, 99.6)
					112 ASN (-37.9, -169.8)
					116 GLU (150.2, -165.2)
					151 HIS (32.9, 78.8)
6	NKG2C	82.0% (50/61)	96.7% (59/61)	2 (0.033)	4 VAL (34.2, 31.5)
					33 LEU (46.3, 87.5)
7	KIR2DS4	90.2% (174/193)	98.4% (190/193)	3 (0.016)	14 PRO (-64.1, -53.5)
					52 ILE (-91.4, 46.7)
					83 VAL (-118.9, -41.0)
8	NCR3	87.3% (96/110)	100.0% (110/110)	0	
9	IL2Rβ	95.3% (183/192)	100.0% (192/192)	0	
10	γc	94.3% (181/192)	100.0% (192/192)	0	
11	IL15Rα	96.9% (63/65)	100.0% (65/65)	0	
12	PILR	94.1% (222/236)	97.9% (231/236)	5 (0.021)	A 2 LEU (-58.8, 30.2)
					A 36 ASN (15.7, 74.4)
					A 61 LYS (-25.5, -53.3)
					B 36 ASN (18.0, 77.2)
					B 61 LYS (-22.2, -59.2)
13	NKG2D	93.1% (229/246)	98.4% (242/246)	4 (0.016)	A 116 GLU (-45.4, 83.0)
					B 132 ALA (172.7, 134.5)
					B 164 GLY (-53.6, 56.7)
					B 176 PRO (-31.6, -74.6)
14	CD16	92.7% (140/151)	100.0% (151/151)	0	
15	KIR2DS1	87.3% (172/197)	95.4% (188/197)	9 (0.046)	65 MET (-52.7, -74.3)
					78 ASP (-22.6, 112.8)
					88 SER (-48.2, 176.4)
					89 ARG (-22.7, 102.0)
					105 THR (-22.4, -53.6)

bioRxiv preprint doi: https://doi.org/10.1101/2020.06.19.160861; this version posted June 20, 2020. The copyright holder for this preprint (which was not certified by peer review) is the author/funder, who has granted bioRxiv a license to display the preprint in perpetuity. It is made available under aCC-BY-NC-ND 4.0 International license.

					107 SER (179.3, 55.2)
					135 PRO (-44.3, -50.9)
					163 GLU (-27.7, 101.6)
					166 ALA (-5.7, -67.1)
16	KIR2DS3	85.8% (169/197)	96.4% (190/197)	7(0.036)	65 THR (-46.5, -75.6)
					78 ASP (-21.0, 113.3)
					89 ARG (-24.8, 104.3)
					107 SER (173.0, 54.7)
					135 PRO (-42.6, -53.0)
					163 GLU (-25.1, 99.9)
					166 ALA (-3.2, -70.1)
17	KIR2DS5	92.2% (178/193)	98.4% (190/193)	3 (0.016)	105 THR (86.7, -37.8)
					188 ASP (92.4, -161.9)
					193 GLY (-56.8, -99.7)
18	NKG2E	86.7% (98/113)	99.1% (112/113)	1(0.009)	149 ASN (61.8, -81.9)

3.1.3 Energy minimization: As two non-bonding atoms in a protein structure approach, an atomic overlap (contact) occurs resulting in Van der Waals repulsion energy greater than 0.3 kcal/mol and subsequently leading to a steric clash. The webserver, *Chiron* is able to resolve severe steric clashes with minimal perturbation of the backbone of the native structure (less than 1 Å Cα RMSD).

Chiron generates a clash score which is a size-independent parameter obtained mathematically by the ratio of total VDW repulsion energy to the total number of contacts. From data generated from high-resolution structures, *Chiron* is able to determine if a protein has artifacts *(*excessive steric clashes) and return the clash score to physiological acceptability (0.02 kcal.mol−1.contact−1) [12].

A reduction in the total van der Waals (VDW) repulsion energy (Kcal/mol) of the clashing atoms. Would lead to a reduction in the steric clashes and consequently improve ligand-binding This is done computationally by rearranging this collection of non-bonding atoms in such a way that their inter-atomic forces are as close to zero as possible [12].

From Table 3, all 17 minimized structures have a physiologically acceptable clash ratio (clash score) of less than 0.02. There is no reduction in the total number of clashes and total VDW repulsion energy (Kcal/mol) in NCR1 and IL2Rγc signifying that these proteins already stable conformations. There is also no reduction in the steric clashes in all the protein structures that were modeled which are KIR2DS1, KIR2DS3, KIR2DS5 and NKG2E. This is because the *SWISS MODEL* webserver during the modeling process repairs distorted geometries or steric clashes through energy minimization [26]. IL2Rβ was not minimized probably due to missing heavy atoms of the backbone [12].

bioRxiv preprint doi: https://doi.org/10.1101/2020.06.19.160861; this version posted June 20, 2020. The copyright holder for this preprint (which was not certified by peer review) is the author/funder, who has granted bioRxiv a license to display the preprint in perpetuity. It is made available under aCC-BY-NC-ND 4.0 International license.

Table 3: Energy Minimization of Protein Structures

S/N	Protein	Structure	Total No. of residues	Total No. of contacts	Total No. of clashes	Total VDW repulsion energy (Kcal/mol)	Clash ratio
1	CD2	Initial	105	1706	131	135.4	0.079
		Final	105	1326	38	21.44	0.016
2	NCR2	Initial	108	1539	55	39.48	0.026
		Final	108	1497	37	26.14	0.017
3	KIR2DS2	Initial	193	2461	79	56.15	0.023
		Final	193	2324	56	35.85	0.015
4	NCR1	Initial	188	2714	84	53.82	0.02
		Final	188	2714	84	53.82	0.02
5	IL2Rα	Initial	123	1520	65	52.26	0.034
		Final	123	1378	39	24.39	0.018
6	NKG2C	Initial	63	788	51	54.34	0.07
		Final	63	701	14	11.35	0.016
7	KIR2DS4	Initial	195	2637	103	85.66	0.032
		Final	195	2398	69	42.26	0.018
8	NCR3	Initial	112	1450	53	38.42	0.026
		Final	112	1394	41	22.95	0.016
9	IL2Rβ	Initial					
		Final					
10	γc	Initial	193	2732	67	39.86	0.015
		Final	193	2732	67	39.86	0.015
11	IL15Rα	Initial	67	847	25	17	0.02
		Final	67	843	25	16.22	0.019
12	PILR	Initial	240	3324	101	66.67	0.02
		Final	240	3402	93	57.85	0.017
13	NKG2D	Initial	250	4424	121	84.66	0.02
		Final	250	4041	115	71.66	0.018
14	CD16	Initial	157	2058	97	79	0.038
		Final	157	2002	54	35.25	0.018
15	KIR2DS1	Initial	199	2507	65	37.54	0.015
		Final	199	2507	65	37.54	0.015
16	KIR2DS3	Initial	199	2452	73	39.33	0.016
		Final	199	2452	73	39.33	0.016
17	KIR2DS5	Initial	195	2281	55	28.65	0.013
		Final	195	2281	55	28.65	0.013
18	NKG2E	Initial	115	1459	27	16.99	0.012
		Final	115	1459	27	16.99	0.012

bioRxiv preprint doi: https://doi.org/10.1101/2020.06.19.160861; this version posted June 20, 2020. The copyright holder for this preprint (which was not certified by peer review) is the author/funder, who has granted bioRxiv a license to display the preprint in perpetuity. It is made available under aCC-BY-NC-ND 4.0 International license.

3.1.4: Validation of docking protocol: 1gya consists of CD2 and N-glycan (alpha-d-mannose, beta-d-mannose and N-acetyl-d-glucosamine) molecules. Figure 1 shows the images of the original 1gya and that of the separated, docked and superimposed. These two closely resemble thereby validating the docking protocol [27].

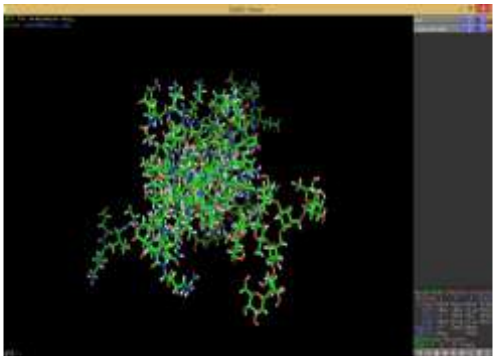

a: Separated, docked & superimposed structure of 1gya

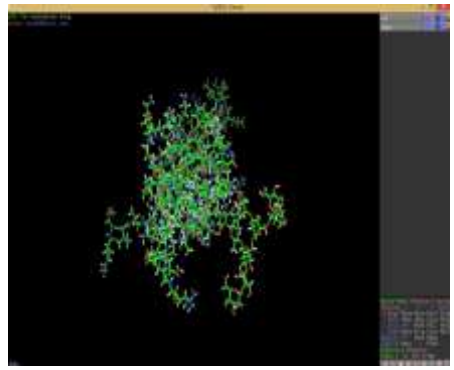

b: Original Structure of 1gya

Figure 1: Separated, docked and superimposed structure of 1gya as compared to the original structure.

3.1.5 Screening for Bioavailability: Prior to docking, a library of 1,697 compounds was screened for bioavailability using the Lipinski and Veber rules. The predictors of good oral bioavailability include number of rotatable bonds, hydrogen bond acceptors (≤ 10), hydrogen bond donors (≤ 5), molecular weight (≤ 500), low polar surface area (TPSA ≤ 140), and lipophilicity (Log P ≤ 5.0) [28, 29]. 1,048 front-runner compounds were selected with zero violations to both rules.

One limitation of the Lipinski rule is the fact that it only applies to compounds that are transported by diffusion through cell membranes. Actively transported compounds are exempted from this rule [30]. The conformational features of these compounds closely resemble endogenous metabolites and as such active transport is enhanced through ATP-dependent mechanisms [31]. This explains why so many proven compounds that have elicited *in vitro* cytotoxicity have been screened out [32].

bioRxiv preprint doi: https://doi.org/10.1101/2020.06.19.160861; this version posted June 20, 2020. The copyright holder for this preprint (which was not certified by peer review) is the author/funder, who has granted bioRxiv a license to display the preprint in perpetuity. It is made available under aCC-BY-NC-ND 4.0 International license.

Table 4: Lead compounds' compliance with Lipinski & Veber rules

	Pubchem ID	MW(g/mol)	Log P	HBD	HBA	TPSA (A²)	No of Rotatable bonds
4'-Methyl-epigallocatechin	176920	320.29	0.3	5	7	120	2
Andrographis Extract	6436016	350.4	2.2	3	5	87	3
Betulalbuside A	14484636	332.39	-0.3	5	7	120	8
Bisabolone Oxide A	91700388	236.35	2.5	0	2	26.3	1
Carveol	7438	152.23	2.1	1	1	20.2	1
cis-Carvotanacetol	12233170	154.25	2.1	1	1	20.2	1
Eugenyl Glucoside	3084296	326.34	0	4	7	109	6
Gibberellin A17	5460657	378.4	0.8	4	7	132	3
Gibberellin A19	5460209	362.4	0.7	3	6	112	3
Gibberellin A20	5280481	332.4	1.2	2	5	83.8	1
Gibberellin A29	5460028	348.4	0.2	3	6	104	1
Gibberellin A44	5460372	346.4	1.6	2	5	83.8	1
Gibberellin A51	443458	332.4	1.7	2	5	83.8	1
Gibberellin A53	440914	348.4	2.2	3	5	94.8	2
Monocrotalline	9415	325.36	-0.7	2	7	96.3	0
Phellandrenol	76373091	152.23	2	1	1	20.2	2
Shikimic Acid	8742	174.15	-1.7	4	5	98	1

bioRxiv preprint doi: https://doi.org/10.1101/2020.06.19.160861; this version posted June 20, 2020. The copyright holder for this preprint (which was not certified by peer review) is the author/funder, who has granted bioRxiv a license to display the preprint in perpetuity. It is made available under aCC-BY-NC-ND 4.0 International license.

3.2 Screening for potency

3.2.1 Binding Affinities: For the purpose of screening, a uniform docking score of -7.0 kcal/mol was chosen as a cut-off value as this depicts strong protein-ligand binding. The choice of a higher docking score would increase the amount of data to be handled and also reduce potency [33]. The binding affinity values reveal the strength of ligand-protein interaction. After docking 1,048 ligands against 18 receptors, 377 front-runner compounds were selected as seen in Table 5 (summary of screening results). This implies that approximately 36% of the screened compounds obtained mainly from fruits, and vegetables have strong binding affinities with the activating receptors of the NK cells. This data further establishes the fact that phytochemicals of fruits, mushrooms and vegetables modulate NK cell activities and thereby promote the prevention of cancer [34].

Table 6 shows the summary of distributions and frequencies of receptor - ligand dockings at frequencies ≤-7.0 kcal/mol. NKG2D, NKG2E and PILR bound with the highest number of ligands in the library. NKG2D is known to be a promiscuous receptor and this suggests why it binds to a high number of ligands in the study [35]. NKG2E which was modeled with a NKG2A template (85.96% similarity) and NKG2D have similar hydrophobicity plots suggesting the possibility of promiscuity. PILR is also known to be a promiscuous type I transmembrane receptor and this suggests why it binds to a high number of ligands in the study [36].

On the contrary, Table 6 also reveals that NCR2, CD2, NKG2C, IL2Rβ and IL15Rα have less than 5%. This is suggestive of the fidelity of these receptors as they specifically bind to only a few ligands [37].

Table 5: Summary of screening results

Total Library of compounds	1697
Bioavailability screening	1048
Docking results cut off	377
Ligand Efficiency Metrics screening	192
Promiscuity and Pharmacokinetics screening	69
Bioactivity screening	17

bioRxiv preprint doi: https://doi.org/10.1101/2020.06.19.160861; this version posted June 20, 2020. The copyright holder for this preprint (which was not certified by peer review) is the author/funder, who has granted bioRxiv a license to display the preprint in perpetuity. It is made available under aCC-BY-NC-ND 4.0 International license.

Table 6: Summary of distributions and frequencies of receptor - ligand dockings (≤ -7.0kcal/mol)

S/N	Receptor	No. of compounds that exceed cut-off	Total No. of docked compounds	Percentage
1	KIR2DS1	75	1048	7.16
2	KIR2DS2	94	1048	8.97
3	KIR2DS3	80	1048	7.63
4	KIR2DS4	84	1048	8.02
5	KIR2DS5	64	1048	6.11
6	NCR1	58	1048	5.53
7	NCR2	13	1048	1.24
8	NCR3	86	1048	8.21
9	PILR	151	1048	14.41
10	CD16A	74	1048	7.06
11	CD2	25	1048	2.39
12	NKG2C	20	1048	1.91
13	NKG2D	235	1048	22.42
14	NKG2E	161	1048	15.36
15	IL2Rα	100	1048	9.54
16	IL2Rβ	36	1048	3.44
17	γc	55	1048	5.25
18	IL15Rα	26	1048	2.48

3.2.2: Ligand Efficiency Metrics: LEM screening identifies compounds with greater potency and ADMET properties [38]. Maintaining the potency of a compound with the right molecular size and lipophilicity is a challenge in multi-parameter lead optimization. It is more ideal to optimize hits with the highest ligand efficiencies than those with the strongest binding affinities [39]. Table 5 reveals that a total of 192 front-runner compounds were obtained after screening using the LEM. The screened compounds had a LE of ≥0.3; an LELP of between -10 and 10; and LLE ≥ 5.0 [39]. Good LE values indicate that compounds have the desired potency at the appropriate weight. With lower molecular weight, there is also room for lead optimization to improve the potency and pharmacokinetic properties [40, 41]

3. 3 QSAR-Based ADMET, Saturation and Promiscuity predictions

As seen in Table 5, a total of 69 front runner compounds emerged from the screening for saturation, promiscuity and pharmacokinetic properties. Many of the eliminated compounds remain viable candidates for lead optimization. Many of the eliminated compounds are also known to have strong antioxidant and immunomodulatory properties.

Molecular complexity which is measured by the carbon bond saturation (fraction of sp^3 carbons - fsp^3) plays a vital role drug discovery. Saturation directly correlates with solubility and saturated hydrocarbons

bioRxiv preprint doi: https://doi.org/10.1101/2020.06.19.160861; this version posted June 20, 2020. The copyright holder for this preprint (which was not certified by peer review) is the author/funder, who has granted bioRxiv a license to display the preprint in perpetuity. It is made available under aCC-BY-NC-ND 4.0 International license.

have stability of the chemical bonds which makes them unreactive [42]. As seen in Table 8, all compounds with values less than 0.25 are unsaturated and therefore eliminated

While drug promiscuity may have its advantage, it elicits undesirable side effects due to ligand interactions with multiple protein targets in the biological system. A good predictor of promiscuity in bioassays is aggregation. Most drugs are not promiscuous even at high concentration. However, some have tendency to self-aggregate in aqueous media. These compounds have disruptive functional groups that can interfere with bioassays by causing activity artifacts leading to false positive results [43]. As seen in Table 8, there are no PAIN (Pan-assay Interference) compounds.

The absorption profile of a drug affects its bioavailability and consequently its efficacy and pharmacological effect [44]. Parameters such as water solubility, Caco-2 cell permeability, Human Intestinal Absorption (HIA), and Skin Permeability are within accepted range [45, 46, 47, 48]. Permeability glycoprotein (P-glycoprotein or Pgp) is a transporter protein that is located on the cell membrane. It is an ATP-dependent efflux pump which flushes out xenobiotics and toxic substances thereby limiting their cellular absorption [49]. From Table 7, all Pgp inhibitors were eliminated to avoid cellular toxicity. However, Pgp inhibitors can be used in overcoming multidrug resistance in cancers or administered with P-gp substrates to overcome the challenges of poor bioavailability associated with the later [50].

The Distribution of a drug determines the pharmacological effect and duration of action. From Table 7, the predicted distribution parameters such as steady state volume of distribution (VDss), Fraction unbound (Fu), Blood Brain Barrier (BBB) permeability and CNS permeability [51] are within pharmacological range

Many drugs that affect CYP450 enzymes by either inducing or inhibiting their activities. CY3A4 is the most abundant isoform in the liver. Inhibiting this enzyme can block it and cause an elevation of levels of substrate leading to toxicity or undesirable pharmacological effects [52, 53, 54]. From Table 8, all CYP450 enzyme inhibitors were eliminated.

The rate at which a drug is excreted determines the dose. Drug excretion is determined by such parameters as total Clearance (CL) which is a total of the renal clearance, hepatic clearance and the lung clearance. From Table 8, all lead compounds CL values within accepted pharmacological range. Human Organic Cation Transporter (OCT2) is a renal uptake transporter protein located on the proximal tubule cells. It removes mostly OCT2 substrates which are mostly cationic drugs from the blood into the urine. The concurrent administration of an OCT2 substrate with an OCT2 inhibitor would lead to a toxic intracellular accumulation of the OCT2 substrate. From Table 8, there is no OCT2 substrate

bioRxiv preprint doi: https://doi.org/10.1101/2020.06.19.160861; this version posted June 20, 2020. The copyright holder for this preprint (which was not certified by peer review) is the author/funder, who has granted bioRxiv a license to display the preprint in perpetuity. It is made available under aCC-BY-NC-ND 4.0 International license.

The toxicity profile of a drug is predicted based on QSAR models such as Microbial and fish toxicity, mutagenicity to *Salmonella typhimurium* (Ames Test), Human ether-a-go-go-related gene (hERG) inhibition, Skin Sensitization, Hepatotoxicity. All lead compounds were non mutagens, non- hERG inhibitors and non-dermatoxic. From Table 9, Eugenyl Glucoside, Gibberellin A19, Gibberellin A51 and Gibberellin A53 are predicted to be hepatotoxic. This implies that they possess structural moieties that could elicit the disruption of normal liver function. This kind of hepatotoxicity usually has a predictable dose-response curve. This suggests that doses below the MTD cannot induce hepatotoxicity [55]. Other dose related toxicity indicators which include Microbial and fish toxicity, Maximum Tolerated Dose (MTD), Acute Toxicity (LD50), and Chronic Toxicity are within acceptable pharmacological range**.**

bioRxiv preprint doi: https://doi.org/10.1101/2020.06.19.160861; this version posted June 20, 2020. The copyright holder for this preprint (which was not certified by peer review) is the author/funder, who has granted bioRxiv a license to display the preprint in perpetuity. It is made available under aCC-BY-NC-ND 4.0 International license.

Table 7: Absorption and Distribution profile of lead compounds

Ligand	H_2 0 Solubility	Caco2 perm.	HIA	Skin Perm	P-gp sub.	P-gp I Inb.	P-gp II Inb.	VDss	Fraction unbound	BBB perm	CNS perm
4'-Methyl-epigallocatechin	-3.09	-0.12	60.73	-2.74	Yes	No	No	1.64	0.26	-0.93	-3.27
Andrographis Extract	-3.49	1.07	95.36	-3.79	No	No	No	-0.29	0.28	-0.6	-2.69
Betulalbuside A	-1.94	-0.14	43.96	-3.03	No	No	No	-0.26	0.65	-1.01	-3.65
Bisabolone Oxide A	-3.63	1.62	96.47	-2.52	No	No	No	0.34	0.43	0.55	-3.05
Carveol	-1.78	1.4	95.18	-2.08	No	No	No	0.17	0.55	0.56	-2.58
cis-Carvotanacetol	-2.15	1.37	95.17	-1.93	No	No	No	0.13	0.47	0.58	-2.12
Eugenyl Glucoside	-1.89	0.58	45.71	-2.87	Yes	No	No	-0.38	0.41	-0.99	-3.73
Gibberellin A17	-2.89	0.82	33.03	-2.74	No	No	No	-0.89	0.42	-0.77	-3.31
Gibberellin A19	-2.81	0.96	47.5	-2.74	No	No	No	-1.6	0.42	-0.68	-3.16
Gibberellin A20	-2.64	1.19	98.91	-2.74	No	No	No	-0.83	0.42	-0.21	-3
Gibberellin A29	-2.66	0.69	71.42	-2.74	No	No	No	-0.82	0.47	-0.6	-3.11
Gibberellin A44	-2.84	1.18	99.3	-2.74	No	No	No	-1.11	0.3	-0.18	-2.29
Gibberellin A51	-2.73	1.14	100	-2.74	No	No	No	-0.97	0.29	-0.09	-2.41
Gibberellin A53	-2.82	0.93	53.27	-2.74	No	No	No	-1.6	0.36	-0.56	-2.31
Monocrotaline	-3.06	0.51	64.76	-3.01	Yes	No	No	0.47	0.74	-0.61	-3.1
Phellandrenol	-1.96	1.49	94.99	-2.33	Yes	No	No	0.22	0.56	0.55	-2.69
Shikimic Acid	-0.52	-0.23	46.68	-2.74	No	No	No	-0.62	0.8	-0.68	-3.58

HIA= Human Intestinal Absorption. Skin Perm = Skin Permeability. P-gp = Plasma glycoprotein. VDSS= Volume of Distribution steady State. BBB= Blood Brain Barrier

bioRxiv preprint doi: https://doi.org/10.1101/2020.06.19.160861; this version posted June 20, 2020. The copyright holder for this preprint (which was not certified by peer review) is the author/funder, who has granted bioRxiv a license to display the preprint in perpetuity. It is made available under aCC-BY-NC-ND 4.0 International license.

Table 8: Metabolism, Excretion, and Saturation and Agglutination profile of lead compounds.

Ligand	CYP2D6 sub	CYP3A4 sub	CYP1A2 inh	CYP2C19 inh	CYP2C9 inh	CYP2D6 inh	CYP3A4 inh	Total Clearance	Renal OCT2 sub	Fraction Csp3	PAINS #alerts
4'-Methyl-epigallocatechin	No	No	No	No	No	No	No	0.35	No	0.25	0
Andrographis Extract	NO	Yes	No	No	No	No	No	1.18	No	0.75	0
Betulalbuside A	No	No	No	No	No	No	No	1.69	No	0.75	0
Bisabolone Oxide A	No	No	No	No	No	No	No	1.13	No	0.8	0
Carveol	No	No	No	No	No	No	No	0.23	No	0.6	0
cis-Carvotanacetol	No	No	No	No	No	No	No	0.19	No	0.8	0
Eugenyl Glucoside	No	No	No	No	No	No	No	0.26	No	0.5	0
Gibberellin A17	No	No	No	No	No	No	No	0.39	No	0.75	0
Gibberellin A19	NO	Yes	No	No	No	No	No	0.47	No	0.75	0
Gibberellin A20	No	Yes	No	No	No	No	No	0.42	No	0.79	0
Gibberellin A29	No	Yes	No	No	No	No	No	0.42	No	0.79	0
Gibberellin A44	No	Yes	No	No	No	No	No	0.36	No	0.8	0
Gibberellin A51	No	Yes	No	No	No	No	No	0.42	No	0.79	0
Gibberellin A53	No	Yes	No	No	No	No	No	0.43	No	0.8	0
Monocrotaline	No	No	No	No	No	No	No	0.73	No	0.75	0
Phellandrenol	No	No	No	No	No	No	No	0.29	No	0.6	0
Shikimic Acid	No	No	No	No	No	No	No	0.69	No	0.57	0

Renal OCT2 = Renal Organic Cation transporter

bioRxiv preprint doi: https://doi.org/10.1101/2020.06.19.160861; this version posted June 20, 2020. The copyright holder for this preprint (which was not certified by peer review) is the author/funder, who has granted bioRxiv a license to display the preprint in perpetuity. It is made available under aCC-BY-NC-ND 4.0 International license.

Table 9: Toxicity profile of lead compounds.

Ligand	AMES toxicity	Max. tolerated dose	hERG I inh	hERG II inh	Oral Rat Acute Toxicity (LD50)	Oral Rat Chronic Toxicity (LOAEL)	Hepatotoxicity	Skin Sensitisation	T.Pyriformis toxicity	Minnow toxicity
4'-Methyl-epigallocatechin	No	0.37	No	NO	2.29	2.93	No	No	0.3	3.75
Andrographis Extract	No	0.13	No	No	2.16	1	No	No	0.49	1.37
Betulalbuside A	No	1.37	No	NO	1.71	3.2	No	No	0.29	3.66
Bisabolone Oxide A	No	0.35	No	No	1.99	1.86	No	Yes	0.73	1.07
Carveol	No	0.84	No	No	1.96	1.89	No	Yes	0.2	1.67
cis-Carvotanacetol	No	0.82	No	No	1.98	1.99	No	Yes	0.32	1.36
Eugenyl Glucoside	No	0.86	No	No	1.95	3.46	Yes	No	0.29	3.8
Gibberellin A17	No	0.44	No	No	2.48	2.7	No	No	0.29	3.1
Gibberellin A19	No	0.4	No	No	2.21	2.28	Yes	No	0.29	2.49
Gibberellin A20	No	0.37	No	No	2.05	2.14	No	No	0.29	1.96
Gibberellin A29	No	0.26	No	NO	2.1	2.5	No	No	0.29	2.69
Gibberellin A44	No	0.15	No	NO	2.06	1.96	No	No	0.29	1.76
Gibberellin A51	No	-0.14	No	NO	2.1	2.36	Yes	No	0.29	1.16
Gibberellin A53	No	0.36	No	No	2.2	2.17	Yes	No	0.29	1.76
Monocrotaline	No	0.42	No	No	2.4	1.99	No	No	0.29	3.88
Phellandrenol	No	0.87	No	No	1.83	1.81	No	Yes	0.09	1.72
Shikimic Acid	No	0.99	No	No	1.16	2.96	No	No	0.26	4.05

hERG = human Ether-a-go-go-related Gene.

bioRxiv preprint doi: https://doi.org/10.1101/2020.06.19.160861; this version posted June 20, 2020. The copyright holder for this preprint (which was not certified by peer review) is the author/funder, who has granted bioRxiv a license to display the preprint in perpetuity. It is made available under aCC-BY-NC-ND 4.0 International license.

3.4 Bioactivity: Affinity does not necessarily predict activity. Binding ligands could be either agonists or competitive inhibitors. Based on a particular drug target, a compound is considered to be active when it's a bioactivity score is more than 0.0; moderately active when score is between −5.0 and 0.0; and inactive when the score is less than −5.0 [56].

Table 10 reveals 17 compounds that are active as nuclear receptor ligands. Many of these compounds are multi-targeted, binding to multiple receptor targets. Bioactivity screening also eliminates promiscuous binding compounds as seen in PILR, NKG2E and NKG2D receptors.

Table 10: Bioactivity profile of front-runner compounds.

S/N	Ligand	GPCR ligand	Ion channel mod.	*Kinase Inh.*	Nuclear Receptor Ligand	Protease Inh.	Enzyme Inh	No of Recep. Targets (≤ -7.0 kcal/mol)
1	Andrographis Extract	0.32	0.17	-0.01	0.94	0.26	0.81	16
2	Gibberellin A53	0.39	0.17	-0.35	0.76	0.18	0.42	6
3	Gibberellin A19	0.32	0.10	-0.30	0.69	0.30	0.43	15
4	Gibberellin A51	0.17	0.21	-0.31	0.67	0.16	0.38	14
5	Gibberellin A44	0.34	0.16	-0.21	0.66	0.19	0.36	16
6	Gibberellin A17	0.36	0.11	-0.25	0.63	0.18	0.33	17
7	Gibberellin A29	0.24	0.20	-0.24	0.60	0.19	0.42	15
8	Gibberellin A20	0.22	0.23	-0.21	0.49	0.09	0.30	7
9	4'-Methyl-epigallocatechin	0.37	0.07	0.11	0.48	0.23	0.39	17
10	Monocrotaline	0.36	0.38	-0.05	0.47	0.50	0.28	7
11	Betulalbuside A	0.27	0.35	-0.05	0.38	0.22	0.73	1
12	Carveol	-0.55	0.14	-1.40	0.25	-0.89	0.23	1
13	Bisabolone Oxide A	-0.11	0.10	-0.97	0.24	-0.35	0.56	1
14	Phellandrenol	-0.75	-0.34	-1.07	0.12	-1.14	0.23	1
15	Eugenyl Glucoside	0.05	-0.03	-0.21	0.02	-0.11	0.32	2
16	Shikimic Acid	-0.38	0.22	-1.13	0.01	-0.37	0.65	1
17	cis-Carvotanacetol	-0.50	0.09	-1.09	0.01	-0.62	0.18	1

3.5 Specificity-Promiscuity Analyses

There is no correlation between potency and specificity. Selectivity plays a strategic role in drug development [57]. Beyond potency, the selectivity of a drug is also important as this guarantees specificity at the biological target reducing unwanted side effects [58].

From Table 11, the comparative analysis of binding affinities shows 6 compounds that have absolute binding specificity with a single receptor (NKG2D or NKG2E) at ≤ -7.0 kcal/mol. Specificity also depicts the strength of interaction between ligand and protein. High chemical specificity means that proteins bind

bioRxiv preprint doi: https://doi.org/10.1101/2020.06.19.160861; this version posted June 20, 2020. The copyright holder for this preprint (which was not certified by peer review) is the author/funder, who has granted bioRxiv a license to display the preprint in perpetuity. It is made available under aCC-BY-NC-ND 4.0 International license.

to a limited number of ligands. This is important as certain physiological processes might require specificity [59, 60]. Compounds such as 4'-Methyl-epigallocatechin, Andrographis Extract, and Gibberellins A17, 19, 29 & 44 have strong binding affinities with 15 and above receptor protein targets.

Table 11: Binding affinities of front runner compounds (post-screening) with cut off value of ≤ -7.0 kcal/mol

S/N	**Compounds**	**Immunoglobulin-like receptors**											**Lectin-like Receptors**			**Others**				
		KIR2DS1	**KIR2DS2**	**KIR2DS3**	**KIR2DS4**	**KIR2DS5**	**NCR1**	**NCR2**	**NCR3**	**PILR**	**CD16A**	**CD2**	**NKG2C**	**NKG2D**	**NKG2E**	**IL2Rα**	**IL2Rβ**	**γc**	**IL15Rα**	**# of targets**
1	4'-Methyl-epigallocatechin	7.1	8.2	7.0	8.1	7.0	8.4	7.5	8.1	7.2	8.0	7.0	*	7.2	8.8	8.9	7.2	8.3	7.6	17
2	Gibberellin A17	8.9	8.3	8.9	9.0	8.6	8.4		8.6	8.8	7.6	7.7	7.3	8.8	7.4	7.7	7.3	7.4	7.1	17
3	Andrographis Extract	8.0	7.1	7.9	7.4	7.6	7.4	*	7.2	8.3	7.7	7.0	7.2	7.4	7.2	7.2	*	7.7	7.2	16
4	Gibberellin A44	8.2	8.4	8.2	8.2	8.1	8.0	*	8.2	8.3	8.0	7.2	7.0	8.0	*	7.3	7.3	7.4	7.0	16
5	Gibberellin A19	8.3	7.5	8.3	8.1	8.3	8.3	*	8.3	8.5	7.4	7.4	7.2	8.4	7.1	7.4	*	7.3	*	15
6	Gibberellin A29	8.2	7.9	8.1	7.7	7.5	7.7	*	8.5	8.7	8.7	7.2	*	7.8	7.7	7.3	7.3	7.6	*	15
7	Gibberellin A51	7.8	8.1	8.0	8.1	7.8	7.5	*	8.5	8.6	8.1	*	7.6	7.7	7.4	7.0	*	7.2	*	14
8	Gibberellin A20	7.4	7.1	7.4	7.0	*	*	*	7.5	7.6	8.2	*	*	*	*	*	*	*	*	7
9	Monocrotaline	7.0	7.3	7.1	*	*	*	*	*	7.5	7.0	*	*	7.1	*	7.0	*	*	*	7
10	Gibberellin A53	*	7.1	*	7.4	7.0	*	*	7.1	7.4	7.2	*	*	*	*	*	*	*	*	6
11	Eugenyl Glucoside	*	*	*	*	*	*	*	*	7.0	*	*	*	*	7.7	*	*	*	*	2
12	Betulalbuside A	*	*	*	*	*	*	*	*	*	*	*	*	*	7.6	*	*	*	*	1
13	Bisabolone Oxide A	*	*	*	*	*	*	*	*	*	*	*	*	*	8.1	*	*	*	*	1
14	Carveol	*	*	*	*	*	*	*	*	*	*	*	*	7.6	*	*	*	*	*	1
15	cis-Carvotanacetol	*	*	*	*	*	*	*	*	*	*	*	*	7.5	*	*	*	*	*	1
16	Phellandrenol	*	*	*	*	*	*	*	*	*	*	*	*	7.8	*	*	*	*	*	1
17	Shikimic Acid	*	*	*	*	*	*	*	*	*	*	*	*	*	7.0	*	*	*	*	1
		9	**10**	**9**	**9**	**8**	**7**	**1**	**9**	**11**	**10**	**6**	**5**	**11**	**10**	**8**	**4**	**7**	**4**	

All binding affinity values are negative.

bioRxiv preprint doi: https://doi.org/10.1101/2020.06.19.160861; this version posted June 20, 2020. The copyright holder for this preprint (which was not certified by peer review) is the author/funder, who has granted bioRxiv a license to display the preprint in perpetuity. It is made available under aCC-BY-NC-ND 4.0 International license.

3.6 Similarity analysis

Structural similarity may suggest closeness in biological activity [61].

3.6.1 Ligand Similarity analyses: As seen in Table 12, a pairwise ligand similarity analyses of Gibberellins A17, A19, A20, A29, A44, A51 and A53 reveal Tanimoto scores ranging from 0.50 to 0.81. Gibberellins A20 and A51 have the same chemical formula but different stereochemistry. Carveol & cis-Carvotanacetol have a Tanimoto score of 0.51. These compounds have been predicted to elicit similar function and would be useful in building pharmacophores for ligand-based drug design [62].

Table 12: Pairwise Ligand Similarity Analysis of active compounds Using Tanimoto Coefficient

		1	**2**	**3**	**4**	**5**	**6**	**7**	**8**	**9**	**10**	**11**	**12**	**13**	**14**	**15**	**16**	**17**
4'-Methyl-epigallocatechin	1	1.00	0.13	0.14	0.07	0.06	0.07	0.25	0.09	0.11	0.09	0.11	0.08	0.11	0.09	0.14	0.10	0.13
Andrographis Extract	**2**	0.13	1.00	0.22	0.22	0.15	0.12	0.18	0.27	0.28	0.27	0.27	0.29	0.28	0.30	0.22	0.09	0.09
Betulalbuside A	**3**	0.14	0.22	1.00	0.12	0.07	0.10	0.37	0.13	0.14	0.16	0.17	0.15	0.16	0.14	0.17	0.11	0.13
Bisabolone Oxide A	**4**	0.07	0.22	0.12	1.00	0.14	0.19	0.19	0.15	0.19	0.21	0.18	0.19	0.19	0.21	0.22	0.16	0.07
Carveol	**5**	0.06	0.15	0.07	0.14	1.00	0.51	0.05	0.07	0.08	0.08	0.08	0.08	0.09	0.09	0.08	0.24	0.14
cis-Carvotanacetol	**6**	0.07	0.12	0.10	0.19	0.51	1.00	0.06	0.06	0.08	0.07	0.07	0.06	0.07	0.09	0.09	0.09	0.09
Eugenyl Glucoside	**7**	0.25	0.18	0.37	0.19	0.05	0.06	1.00	0.08	0.09	0.10	0.12	0.10	0.12	0.08	0.16	0.09	0.13
Gibberellin A17	**8**	0.09	0.27	0.13	0.15	0.07	0.06	0.08	1.00	0.80	0.67	0.60	0.66	0.50	0.75	0.21	0.05	0.09
Gibberellin A19	**9**	0.11	0.28	0.14	0.19	0.08	0.08	0.09	0.80	1.00	0.71	0.63	0.70	0.52	0.80	0.24	0.09	0.10
Gibberellin A20	**10**	0.09	0.27	0.16	0.21	0.08	0.07	0.10	0.67	0.71	1.00	0.79	0.81	0.67	0.75	0.26	0.06	0.10
Gibberellin A29	**11**	0.11	0.27	0.17	0.18	0.08	0.07	0.12	0.60	0.63	0.79	1.00	0.68	0.80	0.67	0.27	0.06	0.11
Gibberellin A44	**12**	0.08	0.29	0.15	0.19	0.08	0.06	0.10	0.66	0.70	0.81	0.68	1.00	0.60	0.74	0.25	0.05	0.10
Gibberellin A51	**13**	0.11	0.28	0.16	0.19	0.09	0.07	0.12	0.50	0.52	0.67	0.80	0.60	1.00	0.55	0.29	0.06	0.10
Gibberellin A53	**14**	0.09	0.30	0.14	0.21	0.09	0.09	0.08	0.75	0.80	0.75	0.67	0.74	0.55	1.00	0.23	0.06	0.10
Monocrotaline	**15**	0.14	0.22	0.17	0.22	0.08	0.09	0.16	0.21	0.24	0.26	0.27	0.25	0.29	0.23	1.00	0.09	0.11
Phellandrenol	**16**	0.10	0.09	0.11	0.16	0.24	0.09	0.09	0.05	0.09	0.06	0.06	0.05	0.06	0.06	0.09	1.00	0.15
Shikimic Acid	**17**	0.13	0.09	0.13	0.07	0.14	0.09	0.13	0.09	0.10	0.10	0.11	0.10	0.10	0.10	0.11	0.15	1.00

bioRxiv preprint doi: https://doi.org/10.1101/2020.06.19.160861; this version posted June 20, 2020. The copyright holder for this preprint (which was not certified by peer review) is the author/funder, who has granted bioRxiv a license to display the preprint in perpetuity. It is made available under aCC-BY-NC-ND 4.0 International license.

3.6.2: Receptor similarity: The multi-target binding of the ligands is likely due to the structural similarities of the protein targets. Empirical evidences show that ligands could have the same binding pocket in different proteins [57]. This may be due to genetic similarities of the proteins. Isoforms of the same protein and those that by co-evolution may exhibit similar biochemical reactions might have the same binding sites [63].

The structural similarity of the target protein was studied using a percent identity matrix in Table 13. Amino acid sequence alignments that produce a pairwise sequence identity >40% is considered high [64]. Out of the 11 members of the Immunoglobulin super family of receptors, KIR2DS1, KIR2DS2, KIR2DS3, KIR2DS4, and KIR2DS5 are highly similar proteins as they have degree of conservation ranging from 86.53-92.65% (Table 13). Of all the 3 lectin-like receptors, consensus sequences only exist between NKG2E & NKG2C with a 90.04% identity. This signifies that these two sets of proteins are isoforms. NKG2E and CD2 have the least identity of 6.36%.

From Figure 2, all the receptors have a common ancestor and have evolutionary relatedness. An original speciation event occurred resulting in three lineages (roots). The tree also depicts the direction of evolution, with the flow of genetic information moving from the roots, through the clades, to the branches, to the taxa and outgroups. Root 3 consists exclusively of the KIR2DS series of receptors. Root 1 Clade 2 also consists of all the lectin-like receptors. Most closely related pairs exist in the sister taxa. KIR2DS1-5 are the most closely related family in all the 18 receptors. The NCR 1-3 are the most divergent.

bioRxiv preprint doi: https://doi.org/10.1101/2020.06.19.160861; this version posted June 20, 2020. The copyright holder for this preprint (which was not certified by peer review) is the author/funder, who has granted bioRxiv a license to display the preprint in perpetuity. It is made available under aCC-BY-NC-ND 4.0 International license.

Table 13: Percent Identity Matrix of Protein Targets

		1	**2**	**3**	**4**	**5**	**6**	**7**	**8**	**9**	**10**	**11**	**12**	**13**	**14**	**15**	**16**	**17**	**18**
NCR2	**1**	100	25.12	15.56	15.38	21.69	12.79	10.26	15.19	17.24	21.57	10.85	17.69	14.29	12.82	12.82	12.82	11.97	11.97
IL15Rα	**2**	25.12	100	15.2	14.09	17.13	14.52	19.64	21.05	10.59	14.65	10.45	13.48	15.13	13.73	13.73	13.73	14.38	13.73
IL2Rα	**3**	15.56	15.2	100	21.08	17.91	11.29	11.27	11.27	13.79	18.09	8.46	9.76	6.57	8.45	7.75	9.15	8.45	8.45
NCR3	**4**	15.38	14.09	21.08	100	26.23	12.16	12.5	12.33	13.57	12.86	9.62	11.58	10.28	12.38	13.33	13.33	15.24	13.33
PILRB	**5**	21.69	17.13	17.91	26.23	100	16.95	12.07	12.07	13.53	12.5	10.16	11.81	12.59	10.42	13.19	11.11	11.81	11.81
NKG2D	**6**	12.79	14.52	11.29	12.16	16.95	100	22.06	22.33	15	15.12	13.21	10.58	13.6	11.11	10.1	11.11	11.11	9.09
NKG2C	**7**	10.26	19.64	11.27	12.5	12.07	22.06	100	90.04	9.49	21.55	8.26	11.21	16.28	17.92	17.92	15.09	19.81	17.92
NKG2E	**8**	15.19	21.05	11.27	12.33	12.07	22.33	90.04	100	8.76	21.16	6.36	11.21	14.73	16.98	16.98	14.15	18.87	16.98
Common γc	**9**	17.24	10.59	13.79	13.57	13.53	15	9.49	8.76	100	22.22	8.43	11.45	9.85	14.75	13.11	13.66	14.21	13.11
IL2Rβ	**10**	21.57	14.65	18.09	12.86	12.5	15.12	21.55	21.16	22.22	100	17.52	18.35	13.28	13.27	14.29	14.29	13.27	13.78
CD2	**11**	10.85	10.45	8.46	9.62	10.16	13.21	8.26	6.36	8.43	17.52	100	18.63	19.07	19.68	20.74	20.21	18.62	19.68
CD16A	**12**	17.69	13.48	9.76	11.58	11.81	10.58	11.21	11.21	11.45	18.35	18.63	100	21.2	19.62	19.14	20.1	20.1	21.53
NCR1	**13**	14.29	15.13	6.57	10.28	12.59	13.6	16.28	14.73	9.85	13.28	19.07	21.2	100	34.76	34.76	34.33	33.91	33.48
KIR2DS4	**14**	12.82	13.73	8.45	12.38	10.42	11.11	17.92	16.98	14.75	13.27	19.68	19.62	34.76	100	89.39	90.2	86.53	86.94
KIR2DS1	**15**	12.82	13.73	7.75	13.33	13.19	10.1	17.92	16.98	13.11	14.29	20.74	19.14	34.76	89.39	100	92.65	91.43	92.24
KIR2DS2	**16**	12.82	13.73	9.15	13.33	11.11	11.11	15.09	14.15	13.66	14.29	20.21	20.1	34.33	90.2	92.65	100	91.84	91.43
KIR2DS3	**17**	11.97	14.38	8.45	15.24	11.81	11.11	19.81	18.87	14.21	13.27	18.62	20.1	33.91	86.53	91.43	91.84	100	92.65
KIR2DS5	**18**	11.97	13.73	8.45	13.33	11.81	9.09	17.92	16.98	13.11	13.78	19.68	21.53	33.48	86.94	92.24	91.43	92.65	100

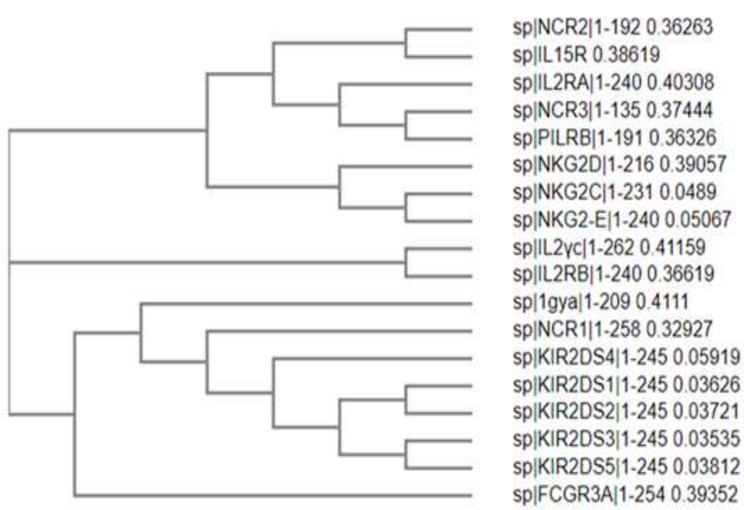

bioRxiv preprint doi: https://doi.org/10.1101/2020.06.19.160861; this version posted June 20, 2020. The copyright holder for this preprint (which was not certified by peer review) is the author/funder, who has granted bioRxiv a license to display the preprint in perpetuity. It is made available under aCC-BY-NC-ND 4.0 International license.

3.7 Binding Site analyses

All residues that are involved in the ligand–protein interactions are located within the extracellular domains of the receptor (See supplementary data). Receptor signaling should commence from the extracellular domain through the helical domain to the cytoplasmic domain.

The greater the number of ligand interactions within the functional domains, the greater the biological activity of the protein is triggered. The 18 receptor targets have functional domains such as Immunoglobulin-like (C and V types), sushi, C- type lectin, and fibronectin type III domains. For example, as seen in supplementary data, Gibberellin A53, 4'-Methyl-epigallocatechin and Gibberellin A51 have all their interactions (hydrophobic and hydrogen bonds) within the C2 type 1 and C2 type 2 domains of the KIR2DS4 receptor (N.B. A value of 5 should be added to all the residue numbers for KIR2DS4 to take care of the rearrangement during energy minimization.)

IL2Rβ has 5 binding sites. Proteins with multiple binding sites show cooperativity. The assembly of the IL2R-IL15R complex allows interfaces between these proteins to create hydrophobic pockets for ligand binding. However, the binding at the original site affects the affinity of all the other sites [65].

3.8: Normal Mode Analysis: Protein flexibility is determined by fluctuations of the alpha carbon atoms of the amino acids. This is seen as rearrangements of side chains or changes in the backbone. Ligand binding induces conformational changes in the protein structure [66]. The stability of protein-ligand complexes would impact on protein function. As revealed in Table 14 structures with the lowest global fluctuation are indicative of the most stable protein-ligand complexes. Ligands of these most stable complexes are the most suitable drug candidates for their respective receptors. The highest numbers of interacting residues are seen in NKG2-D, PILR and NKG2-E which have 32, 26 and 22 residues respectively. The lowest RMSF value is seen in the interaction between IL2Rα and Monocrotalline (0.13), while the highest is between KIR2DS2 and Gibberellin A29 (51.13). The highest number of bonds is seen between PILR and Eugenyl Glucoside (12).

bioRxiv preprint doi: https://doi.org/10.1101/2020.06.19.160861; this version posted June 20, 2020. The copyright holder for this preprint (which was not certified by peer review) is the author/funder, who has granted bioRxiv a license to display the preprint in perpetuity. It is made available under aCC-BY-NC-ND 4.0 International license.

Table 14: Summary of Receptor - Ligand Interactions and RMSF

S/N	Receptor	Total No. of interacting residues	Compounds with highest No. of bonds	Total No. of bonds	Types of bonds	Total RMSF
1	KIR2DS1	14	4'-Methyl-epigallocatechin	9	2	1.62
			Gibberellin A29	8	3	3.63
			Gibberellin A20	7	3	33.92
2	KIR2DS2	19	Gibberellin A51	10	3	18.65
			Monocrotalline	8	3	34.07
			Gibberellin A44	8	2	27.68
3	KIR2DS2	13	4'-Methyl-epigallocatechin	9	2	15.19
			Gibberellin A17	8	3	43.98
			Gibberellin A20	7	3	22.02
			Gibberellin A29	7	3	51.13
4	KIR2DS4	17	Gibberellin A51	8	2	1.47
			4'-Methyl-epigallocatechin	7	2	9.26
			Gibberellin A29	7	2	21.32
			Andrographis Extract	7	2	3.47
5	KIR2DS5	16	Andrographis Extract	10	3	19.16
			Gibberellin A44	9	2	4.8
			Gibberellin A17	5	3	8.29
6	NCR1	11	Gibberellin A51	10	3	46.9
			Gibberellin A19	10	2	20.36
			Gibberellin A44	8	3	29.58
7	NCR2	5	4'-Methyl-epigallocatechin	6	2	15.76
8	NCR3	12	Gibberellin A51	9	3	1.03
			Gibberellin A29	6	3	9.46
			Gibberellin A20	6	2	6.67
9	PILR	26	Eugenyl Glucoside	12	3	0.5
			4'-Methyl-epigallocatechin	11	2	1.34
			Andrographis Extract	10	2	7.78
10	CD16	6	Gibberellin A29	10	2	1.56
			Gibberellin A20	9	2	9.2
			Gibberellin A44	8	2	17.02
11	CD2	6	4'-Methyl-epigallocatechin	9	2	3.1
12	NKG2-C	4	Gibberellin A51	5	2	16.25
13	NKG2-D	32	4'-Methyl-epigallocatechin	11	2	6.55
			Gibberellin A17	10	3	7.13
			Gibberellin A51	9	3	13.15
			Gibberellin A19	9	3	36.43
14	NKG2-E	22	4'-Methyl-epigallocatechin	8	2	29.72
			Betulabuside A	8	2	14.12
			Shikimic acid	6	2	37.47
15	IL2Rα	8	4'-Methyl-epigallocatechin	9	2	4.83
			Monocrotalline	7	2	0.13
16	IL2Rβ	4	4'-Methyl-epigallocatechin	6	2	8.04
17	IL2Rɣ	13	Gibberellin A29	11	3	11.79
			4'-Methyl-epigallocatechin	9	3	1.78
			Gibberellin A44	9	2	2.38
18	IL15Rα	3	4'-Methyl-epigallocatechin	3	2	14.38

The best 3 (or 4) receptor - ligand Interactions were selected as candidates for Normal Mode Analysis.

bioRxiv preprint doi: https://doi.org/10.1101/2020.06.19.160861; this version posted June 20, 2020. The copyright holder for this preprint (which was not certified by peer review) is the author/funder, who has granted bioRxiv a license to display the preprint in perpetuity. It is made available under aCC-BY-NC-ND 4.0 International license.

3.9 Brief review of successful leads

3.9.1: Andrographis Extract obtained from *Andrographis Paniculata* (King of Bitters) has exhibited potent anti-inflammatory and anticancer properties. Its chemo-preventive activity is revealed in the growth suppression of cancer cells by inducing apoptosis and by inhibiting PI3K/AKT, NF-kappa B, and other kinase pathways [67].

In mice, the ethanol extract of *Andrographis paniculata* also significantly induced antibody production and delayed type hypersensitivity response to sheep red blood cells. In terms of nonspecific immune response, the Andrographis extract induced significant immunostimulation as measured by proliferation of splenic lymphocytes, thymocytes and bone marrow cells; the migration of macrophages and phagocytic activity [68,69].

Andrographis paniculata extract is known to be one of the natural products that enhance the efficiency of NK cells in the control of cancer. It promotes NK cell mediated lysis of metastatic tumor cells in mice through an antibody-dependent complement-mediated cytotoxicity [69, 70, 71]. It also significantly increases the production of interleukin-2 and interferon-gamma and decreases pro-inflammatory cytokines such as TNF-α, GM-CSF, IL-1ß, and IL-6 in tumour-bearing animals [69, 70].

3.9.2 – The Gibberellins A17, A19, A20, A29, A44, A51 & A53: Gibberellins (GAs) are a group of closely related plant hormones that regulate several physiological and developmental processes which include germination, elongation, flowering and fruiting [72]. Gibberellins can be obtained from *Abelmoschus esculentus* (Okro) and *Pisum sativum* (Green peas) [73,74].

Gibberellin has been implicated as a modulator of the plant innate immunity. It plays significant role in plant-microbe interaction especially as it has to do with the root's basal defense. Successful fungal colonization is due to altering gibberellin signaling in plants [75]. Gibberellin modulates plant immune system by regulating the Salicylic acid (SA), Jasmonic acid (JA) and Ethylene (ET) signaling systems [76].

There were no direct cytotoxic effects of Gibberellins A17, A19, A20, A29, A44, A51 & A53 found in literature. However, Gibberellin derivatives such as GA-13315 reveal strong antineoplastic effects both *in vitro* and *in vivo*. It inhibits the growth and also accelerates the apoptosis of KB oral cancer cells. GA-13315 also possesses anti-angiogenic properties [77, 78].

GA-13315 inhibits the P-glycoprotein thereby reducing multidrug resistance induced by cancer cells and it also triggers the multidrug resistance-associated Protein -1 [79]. Other synthesized gibberellin derivatives bearing two alpha, beta-unsaturated ketone units showed strong activity in MTT assay against A549, HepG2, HT29, and MKN28 human cancer cell lines. They also

exhibited inhibition to topoisomerase I activity [80].

Gibberellin A4 is known to be a native ligand to the Fab fragment of the haptenic mouse monoclonal antibody, 4-B8 (8)/E9. X ray crystallography of the Fab fragment reveals a typical beta barrel fold which

bioRxiv preprint doi: https://doi.org/10.1101/2020.06.19.160861; this version posted June 20, 2020. The copyright holder for this preprint (which was not certified by peer review) is the author/funder, who has granted bioRxiv a license to display the preprint in perpetuity. It is made available under aCC-BY-NC-ND 4.0 International license.

is a common motif of all immunoglobulins [81]. This suggests why Gibberellins might be able to bind to Immunoglobulin-like receptors which have immunoglobulin domains.

3.9.3 – 4'-Methyl-epigallocatechin: This compound can be found in Locust beans (*Parkia biglobosa*). Epigallocatechin which is found in Green Tea *Camellia sinensis* can also be methylated into 4'-Methyl-epigallocatechin in the human body [82, 83].

Another epigallocatechin derivative such as epigallocatechin gallate (EGCG) which is also found in Green Tea has anticancer effects. Through cell mediated immunity, EGCG reverses myeloid-derived suppressor cell activity [84,85]. ECCG is also able to modulate both the innate and adaptive immune systems. In ameliorating experimental arthritis in mice, it upregulates the Nrf-2 antioxidant pathway, induces Indoleamine-2, 3-dioxygenase (IDO) -producing dendritic cells and increases Treg population [86].

3.9.4 Shikimic Acid is a cyclohexanecarboxylic acid, obtained from *Malus domestica*, Apples. It exhibits anti-inflammatory and antioxidant activities [87,88]. Shikimic acid complex of platinum (II) is active against Leukemia (L1210 and P388) and B 16 Melanoma cell lines [89]. The shikimic acid-based synthesis of zeylenone is widely used as a preparation for chemotherapy in cancer patients [90]. Shikimic acid analogue skeleton is a constituent of several antitumor products [91].

4.0 CONCLUSION

With the aim of triggering cytotoxicity, 1,697 natural compounds derived from 83 plants were docked against 18 activating NKC receptor targets. After rigorous screening, 17 bioactive, non-promiscuous hit compounds with good physicochemical and pharmacokinetic properties were identified.

To add value to the drug discovery process, lead optimization may be necessary in order to adjust the structures of the compounds to achieve stronger binding affinity, greater potency and better ADMET-prediction. The identification of the pharmacophores of strong binding affinity- compounds and the modification of their core structural moieties, could achieve the ideal pharmacokinetic properties.

A further molecular dynamics simulation study is required to confirm the viability of the 18 drug targets. With the right parameterization, the strength and sustainability of the molecular interactions between these proteins and the lead compounds.

bioRxiv preprint doi: https://doi.org/10.1101/2020.06.19.160861; this version posted June 20, 2020. The copyright holder for this preprint (which was not certified by peer review) is the author/funder, who has granted bioRxiv a license to display the preprint in perpetuity. It is made available under aCC-BY-NC-ND 4.0 International license.

5.0 REFERENCES

1. Margret, C.R.; Prabakaran, M.; Jaykar, B.; Venkateswarlu, B.; Palanisamy, P. BRCA mutation: A review of breast cancer. *JDDT*. **2019** 9(2-s), 617-24.
2. WHO. "Cancer Fact Sheet N 297". World Health Organization. February 2018. Retrieved 21 March **2018**.
3. GBD. Mortality and Causes of Death Collaborators. "Global, regional and national life expectancy, all-cause mortality, and cause-specific mortality for 249 causes of death, 1980–2015: a systematic analysis for the Global Burden of Disease Study ". *Lancet.* **2016**, 388 (10053): 1459–1544.
4. Miller, K. Estrogen and DNA Damage: The Silent Source of Breast Cancer? *Journal of the National Cancer Institute*, **2003**, 95(2), 100–102.
5. Jefford, C.; Irminger-Finger, I. Mechanisms of chromosome instability in cancers. *Critical reviews in oncology/hematology*, **2006**, 59, 1-14.
6. Howarth, K.; Blood, K.; Ng, B.; Beavis, J.; Chua, Y.; Cooke, S.; Pole, J.; Chin, S.; Ichimura, K.; Collins, V.P.; Ellis, I.; Caldas, C.; Carter, N.; Edwards, P.A.W.. Chromosome translocations in breast cancer. *Breast Cancer Res.*, **2008**, 10(2), 6.
7. Idowu, M.O.; Powers, C.N. Lung cancer cytology: potential pitfalls and mimics - a review. *Int J. Clin. Exp. Pathol.*, **2010**, 3(4), 367-85.
8. Beatty, L.G.; Whitney, L.G. Immune escape mechanisms as a guide for cancer immunotherapy. *Clin Cancer Res.*, **2015,** 21(4), 687–692.
9. DeLano, W.L. Pymol: An open-source molecular graphics tool. CCP4 *Newsletter On Protein Crystallography*, **2002**, 40: 82-92.
10. Waterhouse, A.; Bertoni, M.; Bienert, S.; Studer, G.; Tauriello, G.; Gumienny, R.; Heer, F.T.; de Beer, T.A.P.; Rempfer, C.; Bordoli, L.; Lepore, R.; Schwede, T. SWISS-MODEL: homology modelling of protein structures and complexes. *Nucleic Acids Res.*, **2018**, 46(1), 296-303.
11. Davis, W.I.; Andrew, L.F.; Vincent, B. C.; Jeremy, N.B.; Gary, J.K.; Xueyi, W.; Laura, W.; Murray, W.; Bryan, A.III; Jack, S.; Jane, S. R.; David, C.R. MolProbity: all-atom contacts and structure validation for proteins and nucleic acids .*Nucleic Acids Research*, **2007**, 35,(suppl_2, 1) : W375–W383.
12. Ramachandran, S.; Kota, P.; Ding, F.; Dokholyan, N.V. Automated minimization of steric clashes in protein structures. *Proteins*, **2011**, 79(1), 261-70.
13. Dallakyan, S.; Olson, A.J. Small-Molecule Library Screening by Docking with PyRx. Methods. *Mol. Biol.*, **2015**, 1263, 243-50.

bioRxiv preprint doi: https://doi.org/10.1101/2020.06.19.160861; this version posted June 20, 2020. The copyright holder for this preprint (which was not certified by peer review) is the author/funder, who has granted bioRxiv a license to display the preprint in perpetuity. It is made available under aCC-BY-NC-ND 4.0 International license.

14. Kim, S.; Thiessen, P.A.; Bolton, E.E.; Chen, J.; Fu, G.; Gindulyte, A.; Han, L.; He, J.; He, S.; Shoemaker, B.A.; Wang, J.; Yu, B.; Zhang, J.; Bryant, S.H. PubChem Substance and Compound databases. *Nucleic Acids Res.*, **2015**, 44(D1), D1202-13.
15. Daina, A.; Michielin, O.; Zoete, V. SwissADME: a free web tool to evaluate pharmacokinetics, drug-likeness and medicinal chemistry friendliness of small molecules. *Scientific reports*, **2017**, 7, 42717.
16. Backman, T.W.; Cao, Y.; Girke, T. ChemMine tools: an online service for analyzing and clustering small molecules. *Nucleic Acids Res.*, **2011**. 39 (Web Server issue), W486-91.
17. Sievers, F.; Wilm, A.; Dineen, D.G.; Gibson, T.J.; Karplus, K.; Li, W.; Lopez, R.; McWilliam, H.; Remmert, M.; Söding, J.; Thompson, J.D.; Higgins, D.G. Fast, scalable generation of high-quality protein multiple sequence alignments using Clustal Omega. *Molecular Systems Biology*, **2011**, 7, 539.
18. Salentin, S. PLIP: fully automated protein-ligand interaction profiler. *Nucl. Acids Res*, **2015**, 43, (W1): W443-W447.
19. Kuriata, A.; Aleksandra, M.; Gierut, T.; Oleniecki, M.P.; Ciemny, A.; Kolinski, M.; Kurcinski, S.K. CABS-flex 2.0: a web server for fast simulations of flexibility of protein structures. *Nucleic Acids Research,* **2018**, 46 (W1), W338–W343.
20. Xiang, Z. Advances in homology protein structure modeling. *Current Protein and Peptide Science*, **2006**, *7*(3), 217-227.
21. Ginalski, K. Comparative modeling for protein structure prediction. *Curr. Opin. Struct. Biol.*, **2006**, 16(2), 172–7.
22. Laskowski, R.A.; MacArthur, M.W.; Moss, D.S. PROCHECK: program to check the stereochemical quality of protein structures. *J. Appl. Cryst.*, **1993**, 26, 283–291.
23. Chen, B.; Vincent, W.; Bryan, A.III, Jeffrey, J.H.; Daniel, A.K.; Robert, M.I.; Gary, J.K.; Laura, W.M.; Jane, S.R.; David, C.R. MolProbity: all-atom structure validation for macromolecular crystallography. *Acta Crystallogr D Biol Crystallogr.*, **2010**, 66(1), 12–21.
24. Subramani, A.; Floudas, C. A. Structure Prediction of Loops with Fixed and Flexible Stems. *J. Phys. Chem. B.*, **2012**, 116(23), 6670–6682.
25. Schneider, M.; Fu, X.; Keating, A.E. X-ray vs. NMR structures as templates for computational protein design. *Proteins: Structure, Function, and Bioinformatics,* **2009**, 77(1), 97-110.
26. Samant, R. L.; Vikrant, C.S.; Abhay, C. Online Servers and Offline Tools for Protein Modelling, Optimization and Validation: A Review. *Int. J. Pharm. Sci. Rev. Res.,* **2014**, 28(1): 123-127.
27. Mukherjee, S.; Balius, T.E.; Rizzo, R.C. Docking validation resources: protein family and ligand flexibility experiments. *Journal of chemical information and modeling,* **2010**, 50(11), 1986-2000.

bioRxiv preprint doi: https://doi.org/10.1101/2020.06.19.160861; this version posted June 20, 2020. The copyright holder for this preprint (which was not certified by peer review) is the author/funder, who has granted bioRxiv a license to display the preprint in perpetuity. It is made available under aCC-BY-NC-ND 4.0 International license.

28. Lipinski, C.A. Lead- and drug-like compounds: the rule-of-five revolution. *Drug Discovery Today: Technologies*, **2004**, 1(4), 337–341.
29. Veber, D.F.; Johnson, S.R.; Cheng, H.Y.; Smith, B.R.; Ward, K.W.; Kopple, K.D. Molecular properties that influence the oral bioavailability of drug candidates. *J. Med. Chem.*, **2002**, 45(12), 2615-23.
30. Zhang, M.Q.; Wilkinson, B. Drug discovery beyond the 'rule-of-five'. *Curr. Opin. Biotechnol.*, **2007**, 18(6), 478-88.
31. Ganesan, A. The impact of natural products upon modern drug discovery. *Curr. Opin. Chem. Biol.*, **2008**, 12(3), 306-17.
32. Huggins D. J.; Ashok, R.V.; David, R. Rational Methods for the Selection of Diverse Screening Compounds. *ACS Chem. Biol.*, **2011**, 6(3), 208–217.
33. Hopkins, A.L. *Pharmacological Space in the Practice of Medicinal Chemistry,* 4th ed.; Elsevier: USA, **2008**.
34. Kim, Y.S.; Thomas, J.S.; Nancy, H.C.; John, A.M.; Howard, A.Y. Impact of Dietary Components on NK and Treg Cell Function for Cancer Prevention. *Mol. Carcinog.*, **2015**, 54(9), 669–678.
35. Petrie, E.J.; Clements, C.S.; Lin, J.; Sullivan, L.C.; Johnson, D.; Huyton, T.; Heroux, A.; Hoare, H.L.; Beddoe, T.; Reid, H.H.; Wilce, M.C.; Brooks, A.G.; Rossjohn, J. CD94-NKG2A recognition of human leukocyte antigen (HLA)-E bound to an HLA class I leader sequence. *J, Exp. Med.*, **2008**, 205(3), 725-35.
36. Vlieg, H.C.; Huizinga, E.G.; Janssen, B.J.C. Structure and flexibility of the extracellular region of the PirB receptor. *J. Biol. Chem*., **2019**, 294:4634-4643.
37. Attie, A.D.; Ronald, T.R. Analysis of Receptor–Ligand Interactions. *J. Chem. Educ*. **1995**, 72(2), 119–124.
38. Tarcsay, A.; Nyiri, K.; Keserű, G.M. Impact of Lipophilic Efficiency on Compound Quality. *J. Med. Chem*., **2012**, 55, 1252−1260.
39. Hopkins, A. L.; Groom, C.R.; Alex, A. Ligand efficiency: a useful metric for lead selection. *Drug Disc. Today*, **2004**, 9(10), 430-431.
40. Zhu, T.; Shuyi, C.; Pin-Chih, S.; Ram, Patel.; Darshan, S.; Heta, B.C.; Richard, S.; Michael, E. J.; Kirk, E.H. Hit Identification and Optimization in Virtual Screening: Practical Recommendations Based Upon a Critical Literature Analysis. *J. Med. Chem.*, **2013**, 56(17), 6560–6572.
41. Murray, C .W.; Daniel, A. E.; Andrew, L.H.; György, M.K.; Paul, D.L.; David, C.R.; Charles, H.R.; Nicola, J.R. Validity of Ligand Efficiency Metrics. *ACS Med. Chem. Lett.,* **2014**, 5(6), 616–618.

bioRxiv preprint doi: https://doi.org/10.1101/2020.06.19.160861; this version posted June 20, 2020. The copyright holder for this preprint (which was not certified by peer review) is the author/funder, who has granted bioRxiv a license to display the preprint in perpetuity. It is made available under aCC-BY-NC-ND 4.0 International license.

42. Lovering, F.; Bikker, J.; Humblet, C. Escape from flatland: increasing saturation as an approach to improving clinical success. *J. Med. Chem.*, **2009**, 52(21), 6752-6.
43. Bajoratha, J.. Activity artifacts in drug discovery and different facets of compound promiscuity. *F1000Res*., **2014**, 3, 233.
44. Dhillon, B.; Narendra, K.G.; Rishabha, M.; Pramod, K.S. Poorly Water Soluble Drugs: Change in Solubility for Improved Dissolution Characteristics a Review. *Global Journal of Pharmacology*, **2014**, 8(1), 26-35.
45. Szisz, D.; Antal, L. Solubility prediction - ChemAxon's Solubility Predictor. https://chemaxon.com/news/solubility-prediction-chemaxons-solubility-predictor (Accessed **2018**).
46. van Breemen, R.B.; Li, Y. Caco-2 cell permeability assays to measure drug absorption. *Expert Opin. Drug Metab. Toxicol.,* **2005**, 1(2), 175-85.
47. Zhao, Y.H.; Le, J.; Abraham, M.H.; Hersey, A.; Eddershaw, P.J.; Luscombe, C.N.; Butina, D.; Beck, G.; Sherborne, B.; Cooper, I.; Platts, J.A. Evaluation of human intestinal absorption data and subsequent derivation of a quantitative structure-activity relationship (QSAR) with the Abraham descriptors. *J. Pharm. Sci.,* **2001**, 90(6), 749-84.
48. Yee, S. In vitro permeability across Caco-2 cells (colonic) can predict in vivo (small intestinal) absorption in man--fact or myth. *Pharm Res*., **1997**, 14 (6), 763-6.
49. Amin, M.L. P-glycoprotein Inhibition for optimal drug delivery. *Drug Target Insights*, **2013,** 7, 27-34.
50. Chung, F.S.; Jayson, S.S.; Miguel, Francisco, M.D.J.; Camille, V.T.; Melvin, F.E.S. Disrupting P-glycoprotein function in clinical settings: what can we learn from the fundamental aspects of this transporter? *Am. J. Cancer. Res.,* **2016**, 6(8), 1583–1598.
51. Scheife, R.T. Protein Binding: What Does It Mean? *Annals of Pharmacotherapy*. **1989**, 23(7-8): S27-S31.
52. Lewis, D.F. Human cytochromes P450 associated with the phase 1 metabolism of drugs and other xenobiotics: a compilation of substrates and inhibitors of the CYP1, CYP2 and CYP3 families. *Curr. Med. Chem.,* **2003**, 10, 1955-72.
53. Guengerich, F.P. Common and uncommon cytochrome P450 reactions related to metabolism and chemical toxicity. *Chem. Res. Toxicol.,* **2001**, 14, 611-50.
54. Thummel, K.E.; Wilkinson, G.R. *In vitro* and *in vivo* drug interactions involving human CYP3A. *Annu. Rev. Pharmacol. Toxicol.,* **1998**, 38: 389430.
55. Pirmohamed, M.; Breckenridge, A.M.; Kitteringham, N.R.; Park, B.K. Adverse drug reactions. *BMJ.*, **1998**, 316(7140), 1295–8.
56. Khan, T.; Shalini, D.; Rumana, A.; Saman, R.; Iqbal, A; Seema, J.; Abdul, R.K. Molecular docking, PASS analysis, bioactivity score prediction, synthesis, characterization and biological

bioRxiv preprint doi: https://doi.org/10.1101/2020.06.19.160861; this version posted June 20, 2020. The copyright holder for this preprint (which was not certified by peer review) is the author/funder, who has granted bioRxiv a license to display the preprint in perpetuity. It is made available under aCC-BY-NC-ND 4.0 International license.

activity evaluation of a functionalized 2-butanone thiosemicarbazone ligand and its complexes. *J. Chem. Biol.*, **2017**, 10(3), 91–104.

57. Sturm, N.; Desaphy, J.; Quinn, R.J.; Rognan, D.; Kellenberger, E. Structural insights into the molecular basis of the ligand promiscuity. *J. Chem. Inf. Model*, **2012**, 52(9), 2410-21.
58. Guo, Z.R. Drug promiscuity. *Yao Xue Xue Bao*., **2011**, 46(4), 361-9.
59. Eaton, B.E.; Gold, L.; Zchi, D.A. Let's get specific: the relationship between specificity and affinity. *Chemistry & Biology*. **1995**, 2 (10), 633–638.
60. Tanford, C. Chemical basis for antibody diversity and specificity". *Accounts of Chemical Research*. **1968**, 1(6), 161–167.
61. Kubinyi, H. Chemical Similarity and Biological Activities. *J. Braz. Chem. Soc*., **2002**, 13(6), 717-726.
62. Acharya, C.; Coop, A; Polli, J.E.; Mackerell, A.D. Jr. Recent advances in ligand-based drug design: relevance and utility of the conformationally sampled pharmacophore approach. *Curr. Comput. Aided Drug Des.*, **2011**, 7(1), 10-22.
63. Yeang, C.; Haussler, D. Detecting Coevolution in and among Protein Domains. *PLoS Comput Biol*., **2007**, 3(11), 211.
64. Rost, B. Twilight zone of protein sequence alignments. *Protein Eng*., **1999**, 12, 85–94.
65. Stauber, D.J.; Debler, E.W.; Horton, P.A.; Smith, K.A.; Wilson, I.A. Crystal structure of the IL-2 signaling complex: paradigm for a heterotrimeric cytokine receptor. *Proc. Natl. Acad. Sci., USA*, **2006**, 103(8), 2788-93.
66. Najmanovich, R.; Josef, K.; Vladimir, S.; Marvin, E. Side-chain flexibility in proteins upon ligand binding. *PROTEINS: Structure, Function, and Genetics*, **2000**, 39, 261–268.
67. Mishra, S.K.; Tripathi, S.; Shukla, A.; Oh, S.H.; Kim, H.M. Andrographolide and analogues in cancer prevention (Elite Ed). *Front Biosci.*, **2015**, 7, 255-66.
68. Puri, A.; Saxena, R.; Saxena, R.P.; Saxena, K.C.; Srivastava, V.; Tandon, J.S. Immunostimulant agents from *Andrographis paniculata*. *J. Nat. Prod*., **1993**, 56(7), 995-9.
69. Sheeja, K.; Kuttan, G. Modulation of natural killer cell activity, antibody-dependent cellular cytotoxicity, and antibody-dependent complement-mediated cytotoxicity by andrographolide in normal and Ehrlich ascites carcinoma-bearing mice. *Integr. Cancer Ther.*, **2007**, 6(1), 66-73.
70. Sheeja, K.; Kuttan, G. *Andrographis paniculata* downregulates proinflammatory cytokine production and augments cell mediated immune response in metastatic tumor-bearing mice. *Asian Pac. J. Cancer Prev.*, **2010**, 11(3), 723-9.
71. Nouroz, F.; Farzana, B.; Shumaila, N.; Nosheen, M. Natural killer cells enhance the immune surveillance of cancer. *Egyptian Journal of Medical Human Genetics*. **2016**, 17 (2): 149-154.
72. Hedden, P.; Sponsel, V. A Century of Gibberellin Research. *J. Plant Growth Regul.*, **2015**, 34(4), 740-60.

bioRxiv preprint doi: https://doi.org/10.1101/2020.06.19.160861; this version posted June 20, 2020. The copyright holder for this preprint (which was not certified by peer review) is the author/funder, who has granted bioRxiv a license to display the preprint in perpetuity. It is made available under aCC-BY-NC-ND 4.0 International license.

73. Koshioka, M.T.; Nishijima, H.Y. Endogenous gibberellins in the immature seeds of okra (*Abelmoschus esculentus*). *Journal of Plant Physiology*, **1996**, 149 (1–2), 129-132.
74. Yu-xian, Z.; Davies, P.J.; Halinska, A. Metabolism of Gibberellin A12 and A12-Aldehyde in Developing Seeds of *Pisum sativum* L.' *Plant Physiol.*, **1991**, 97, 26-33.
75. Scha¨fer, P.; Stefanie, P.1.; Lars, M.; Doreen, Z.; Peter, M.; Chandler, F.W.; Uwe, S.; Jo¨ rn Pons-Ku¨, H.; Sophia, S.; Uwe, S.; Karl-Heinz, K. Manipulation of plant innate immunity and gibberellin as factor of compatibility in the mutualistic association of barley roots with *Piriformospora indica. The Plant Journal.* **2009**, 59, 461–474.
76. Vidhyasekaran, P. Plant Hormone Signaling Systems in Plant Innate Immunity. Part of the Signaling and Communication in Plants book series. *SIGCOMM*, **2014**, 2, 383-401.
77. Zhang, Y.; Hui, Z.; Jingbo, C.; Haixia, Z.; Xianghui, Z.; Hongbin, Z.; Chen, Q. Antitumor and antiangiogenic effects of GA-13315, a gibberellin derivative. *Investigational New Drugs,* **2012**, 30(1), 8–16.
78. Shen, S.; Tang, J. Effects and mechanism of GA-13315 on the proliferation and apoptosis of KB cells in oral cancer. *Oncology Letters*, **2017**, 14(2),1460-1463.
79. Mo, J.; Kang, M.; Ye, J.X.; Chen, J.B.; Zhang, H.B.; Qing, C. Gibberellin derivative GA-13315 sensitizes multidrug-resistant cancer cells by antagonizing ABCB1 while agonizes ABCC1. *Cancer Chemother Pharmacol.,* **2016**, 78(1), 51-61.
80. Chen, J.; Sun, Z.; Zhang, Y.; Zeng, X.; Qing, C.; Liu, J.; Li, L.; Zhang, H. Synthesis of gibberellin derivatives with anti-tumor bioactivities. *Bioorg. Med. Chem. Lett.,* **2009**, 19(18), 5496-9.
81. Murata, T.; Fushinobu, S.; Nakajima, M.; Asami, O.; Sassa, T.; Wakagi, T.; Yamaguchi, I. Crystal structure of the liganded anti-gibberellin A (4) antibody 4-B8(8)/E9 Fab fragment. *Biochem. Biophys. Res. Commun.,* **2002**, 293(1), 489-96.
82. Tringali, C.; Carmela, S.; Onofrio, D.L. Bioactive constituents of the bark of *Parkia biglobosa. Fitoterapia.* **2000**, 71(2), 118–125.
83. Yashi, A.Y.; Boris, V.N.; Emilie, C.; Yakov, I.Y. Determination of the Chemical Composition of Tea by Chromatographic Methods: A Review. *Journal of Food Research*, **2015**, 4(3).
84. Khan, N.; Mukhtar, H. Multitargeted Therapy of Cancer By Green Tea Polyphenols. *Cancer Lett.,* **2008**, 269(2), 269–280.
85. Orentas, R.J. Reading the tea leaves of tumor-mediated immunosuppression. *Clin Cancer Res*.**2013**. Clin Cancer Res. 2013 Mar 1; 19(5): 955–957.
86. So-Youn, M.; Mei, Y.; Sang, B.K.; Sneha, R.; Seong-Ryuel, K.; Kamala, Vanarsa.; Ho-Youn, K.; Laurie, S.D. Green Tea Epigallocatechin-3-Gallate Suppresses Autoimmune Arthritis Through Indoleamine-2,3-Dioxygenase Expressing Dendritic Cells and the Nuclear Factor, Erythroid 2-Like 2 Antioxidant Pathway. *Journal of Inflammation,* **2015**, 12, 53.

bioRxiv preprint doi: https://doi.org/10.1101/2020.06.19.160861; this version posted June 20, 2020. The copyright holder for this preprint (which was not certified by peer review) is the author/funder, who has granted bioRxiv a license to display the preprint in perpetuity. It is made available under aCC-BY-NC-ND 4.0 International license.

87. Chen, X.; Li, X.; Zhai, X.; Zhi, X.; Cao, L.; Qin, L.; Su, J. Shikimic Acid Inhibits Osteoclastogenesis in Vivo and in Vitro by Blocking RANK/TRAF6 Association and Suppressing NF-κB and MAPK Signaling Pathways. *Cell Physiol. Biochem.*, **2018**, 51, 2858–2871.

88. Hulme, A.C. Shikimic Acid in Apple Fruits. *Nature*, **1956**, 178(4540), 991-992.

89. Farrell, N.; Roberts, J.D.; Hacker, M.P. Shikimic acid complexes of platinum. Preparation, reactivity, and antitumor activity of (R,R-1,2-diaminocyclohexane) bis(shikimate) platinum (II). Evidence for a novel rearrangement involving platinum-carbon bond formation. *J Inorg Biochem*., **1991**, 42(4), 237–246.

90. Zhang, Y.; Liu, A.; Ye, Z.G.; Lin, J.; Xu, L.Z.; Yang, S.L. New approach to the total synthesis of (-)-zeylenone from shikimic acid. *Chem Pharm Bull*., **2006**, 54:1459. doi: 10.1248/cpb.54.1459.

91. Sánchez-Abella, L.; Fernández, S.; Armesto, N.; Ferrero, M.; Gotor, V. Novel and efficient syntheses of (-)-methyl 4-epi-shikimate and 4,5-epoxyquinic and -shikimic acid derivatives as key precursors to prepare new analogues. *J. Org. Chem*., **2006**, 71(14), 5396–5399.